Stabilization of magnetic repulsive levitation system by superconducting magnetic bearing

Zhao Yiming [a], Iwanori Murakami [a], Makoto Shimizu [a], Reymond Chi[a], Yoshinori Ando

[a] Gunma University,1-5-1 Tenjin, Kiryu, Gunma, Japan, t171b606@gunma-u.ac.jp

***Abstract*—In this research, we invented and produced a Superconducting magnetic bearing using repulsive permanent magnet. The repulsive magnetic levitation system with permanent magnet can generate strong levitation force without power supply. However, it is unstable except in the repulsion direction. In contrast, superconducting magnetic bearings can generate restoring force in all directions by utilizing the property of magnetic flux pinning of superconductors.**

Therefore, we constructed a superconducting magnetic bearing (SMB) which is stable in all axis without control and has a strong axial levitation force by combining a repulsive type magnetic levitation system and a superconducting magnetic levitation system.

Furthermore, the driving test of the flywheel incorporating the SMB was carried out to verify the characteristics of the SMB. As a result of the experiment, it was confirmed that the flywheel could overcome the resonance and drive it. The maximum rotation speed of the flywheel was 10000[rpm].

I. INTRODUCTION

Superconducting Magnetic Bearing (SMB) used for the magnetic levitation flywheel utilizes the fact that the magnet can be constrained in a noncontact manner in the space by magnetic flux pinning which is one of characteristics of the second kind superconductor. Rotational loss occurs in bearings such as metal bearings and rolling bearings, which are subject to contact, and when used for a long time, the function is deteriorated by abrasion. SMB generates restoring force in all axes without control, it is not necessary to lubricate and the rolling loss can be made extremely low. Further, it is possible to realize a bearing having high rigidity only in a specific direction and a soft bearing in the other direction. Therefore, it is suitable for high-speed rotation and it is expected to have a semi-permanent life. With this feature, researches on storage of electricity by a flywheel of a high temperature superconducting levitation motor and centrifugal separator are being made.

Previously, this research team developed an SMB that supports repulsive magnetic levitation [16], but the force due to magnetic flux pinning of the superconductor was the main body of the axial restoring force to the end.

Here, considering the case of supporting the load due to axial gravity by passive magnetic bearings with permanent magnets for use as the bearings of the flywheel, in the case of the suction type, since the restoring force constantly acts in the direction perpendicular to the suction direction, it is stable However, in the repulsive type, the repulsive force becomes stronger as it approaches the repulsion direction, so the repulsive force becomes stronger, so it is stable in the repulsion direction, but in the direction orthogonal to the repulsion direction Including pitching is unstable. However, if this unstable force can be canceled in some way, a strong restoring force can be obtained without a power supply by a strong magnetic force by the rare earth magnet.

Therefore, in this study, we take advantage of permanent strong levitating force without power supply of repulsion levitation system by permanent magnet and take advantage of the repulsive force of permanent magnet for the axial levitation force required for flying the flywheel, we aim to stabilize only the radial instability generated by the magnet by the flux pinning of the superconductor.

We measure the restoring forces in the radial, axial and pitching directions of the produced magnetic bearings and verify the usefulness of the SMB stabilization method of the repulsive magnetic levitation system proposed in this research.

In addition, we fabricated a flywheel incorporating the bearing part we made this time, and confirmed the usefulness of SMB manufactured by driving experiment.

II. DEVELOPMENT OF SUPERCONDUCTING MAGNETIC BEARING (SMB)

2.1 Configuration of SMB

As shown in Fig.2.1, a ring magnet magnetized in the radial direction is realized in a pseudo manner by adopting a configuration in which a segment type magnet magnetized at the rotor side in the rotor side is combined with a ferrous iron pipe type part I thought about doing it. This uses 16 segmented magnets of outer N pole magnetization, pipe shaped iron plate, 16 segmented magnets of outer S pole magnetization.

In this configuration, there are two magnetic flux converging parts in the cross section, and when the displacement is applied to the PM in the radial direction (horizontal direction), the direction and strength of the magnetic flux entering the high temperature superconductor (HTS) greatly changes. Therefore, we thought that the restoring force in the radial direction could be improved.

First of all, SMB with the structure as shown in Fig.2.2 was devised and manufactured. By placing two ring-shaped permanent magnets with magnetization in the thickness direction on the outside of the unit shown in Fig. 2.1 on the stator side and the rotor side, a magnetically repulsive levitation part by a permanent magnet is constituted.

Actually, when SMB having this structure was manufactured, although the magnetic flux density was obtained according to the simulation beforehand, the restoring force by the HTS was insufficient so that the unstable force generated by the repulsive magnet could not be canceled out.

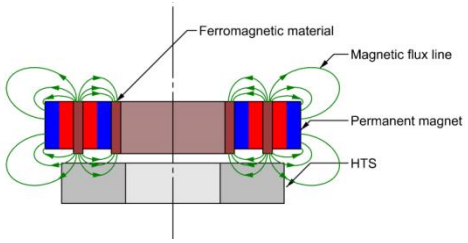

Fig.2.1 Rotor magnet configuration with magnetic flux convergence

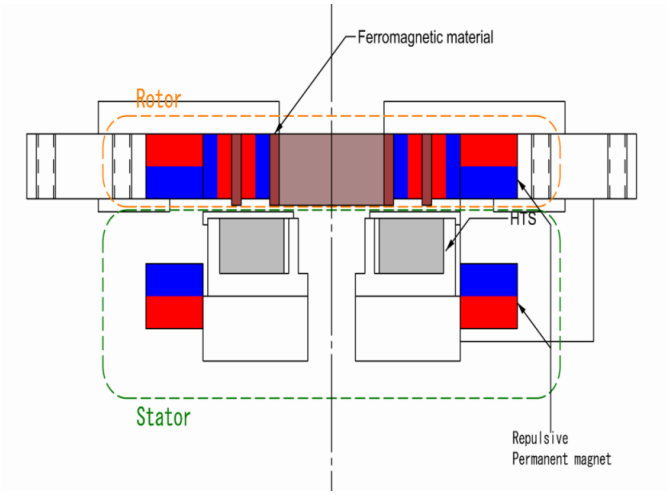

Fig.2.2 HTS Magnet configuration with repulsive permanent magnet

Therefore, in order to strengthen the restoring force by magnetic flux pinning, we also decided to utilize the aspect of HTS. The magnetic flux converging part is constituted by arranging the stations of the ring type permanent magnet of the thickness direction magnetization facing each other and sandwiching the ferromagnetic ring shaped disc thereon to the outside of the unit shown in Fig.2.2, A strong magnetic flux density is generated in the radial direction at the side surface portion.

Then, in order to generate an axial restoring force for supporting the gravity acting on the flywheel, by arranging the same as the ring type permanent magnet on the rotor side on the stator side so as to repel the lower side thereof, the magnetic repulsive portion.

The repulsive force by this permanent magnet also works in the radial direction, so it becomes unstable in the radial direction. Since this repulsive force is thought to increase in inverse proportion to the square of the distance as the distance between the permanent magnets approaches, by adjusting the distance of the permanent magnet repulsion part finely, the radial unstable force can be restrained by the binding force by the superconductor So that it is within the range that can be stabilized.

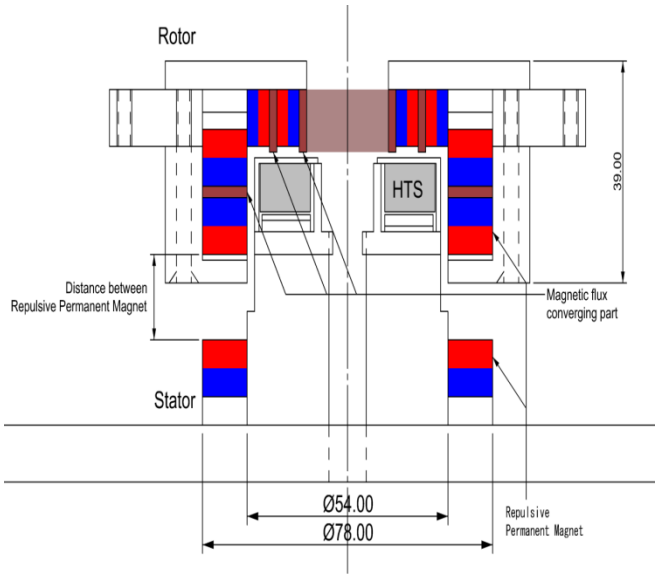

Fig.2.3 HTS Magnet configuration with repulsive permanent magnet

Fig.2.3 shows the final SMB structure of this study combining the axial flux convergence part for HTS pinning, radial flux convergence part and levitation force generation repulsion magnet part.

2.2 Specifications of superconductor

The specifications of HTS used in this research are shown in Table 2.1. The appearance is shown in Fig.2.4. Superconducting bulk material (QMG®) made by Nippon Steel Sumikin.

Table 2.1 Specifications of the HTS

Material composition	Gd-Ba-Cu-O type
Maker	NIPPON STEEL &SUMITOMO METAL CORPORATION
Outside diameter	47 [mm]
Inside diameter	20 [mm]
Height	8 [mm]

Fig.2.4 Photograph of HTS

III. MEASUREMENT AND ANALYSIS

3.1 Magnetic flux density distribution generated by the SMB rotor section

As mentioned above, in this study, the magnetic arrangement of the SMB rotor section is formed by combining the pipe type ferromagnetic body and the segment type magnet of the radial magnetization to generate a large magnetic flux density gradient in the radial direction I made it. In the magnetic flux converging part, a thin ferromagnetic substance plate is sandwiched between the segment magnet with the N pole on the radially outer side and the N pole on the inside, and the ferromagnetic plate is magnetized strongly, so that the magnet creates Due to the synergistic effect with the magnetic field, high magnetic flux density is generated at the end face of the ferromagnetic material.

The magnetic flux density distribution generated by this structure on the HTS surface part was confirmed by simulation using electromagnetic analysis software, and it was confirmed by actually manufacturing the rotor part and measuring the magnetic flux density.

3.1.1 The simulation of magnetic flux density

We simulated the magnetic flux density distribution generated by the SMB permanent magnet of this study by electromagnetic analysis software JMAG using the finite element method. The model used for the simulation is shown in Fig.3.1.

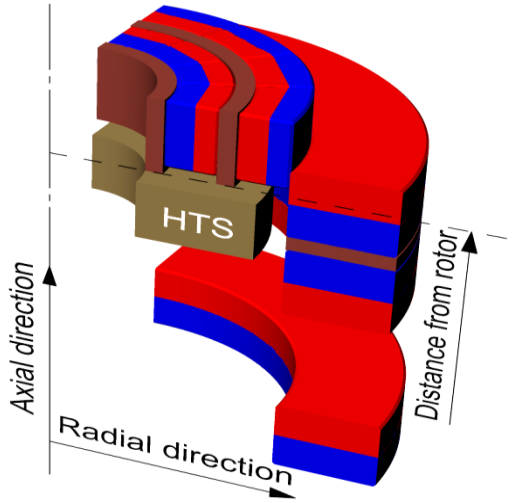

Fig.3.1 1/4 cut model for simulation

The graph of the magnetic flux density on the upper surface of the HTS was plotted at the distance from the lower end of the rotor section, 1 to 6 [mm]. The plot section was set in the position shown in the Fig.3.2. Similarly, the graph of the magnetic flux density on the side of the HTS was plotted with the radius R22 to R26 [mm] from the rotation axis. The plot section was set in the position shown in the Fig.3.3.

3.1.2 The measurement of magnetic flux density

As shown in Fig.3.4, the SMB was fixed in the state of being turned upside down, and the magnetic flux density measuring probe with the Hall element was used, and this was fixed by moving it on the stage and moved. Depending on the structure of the magnetic flux density measuring probe, there are sections which are plotted in the simulation but cannot be measured.

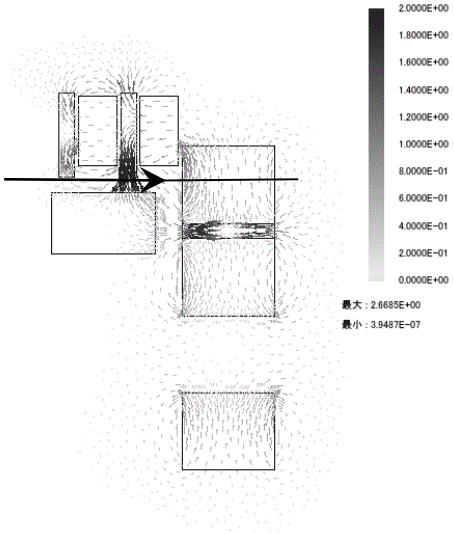

Fig.2.6 Plot section line at top of HTS

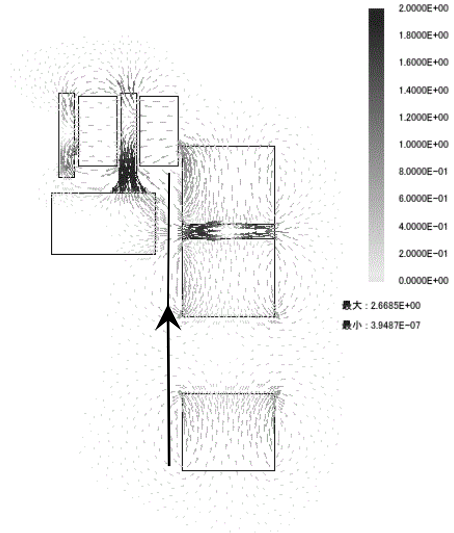

Fig.3.3 Plot section line of magnetic flux density at side of HTS

A graph obtained by plotting the result of measurement of magnetic flux density and simulation result is shown below. A graph of the radial component of the upper surface of the HTS is shown in Fig.3.5, and a graph of the axial direction component is shown in Fig.3.6 A graph of the radial component of the side of HTS is shown in Fig.3.7, and a graph of axial component is shown in Fig.3.8. Since there is no repulsive permanent magnet on the stator side at the time of measurement, it is slightly different from the simulation result of the previous section.

For the radial direction component of the measurement results on the HTS top surface, the simulation result and the measurement result almost agree. For the axial direction component, the measurement result is slightly smaller toward the minus side as a whole than the simulation result.

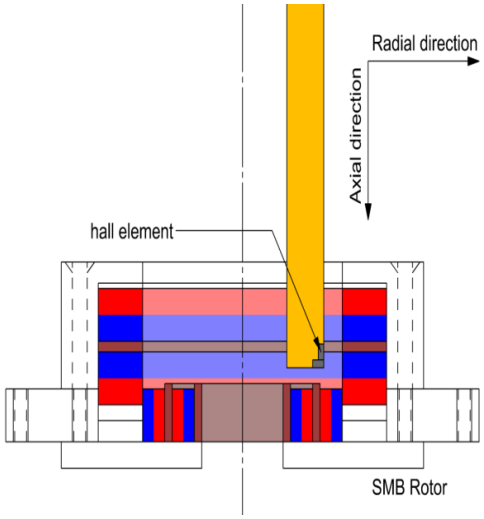

Fig.3.4 Measuring method of magnetic flux density of SMB rotor (upside down)

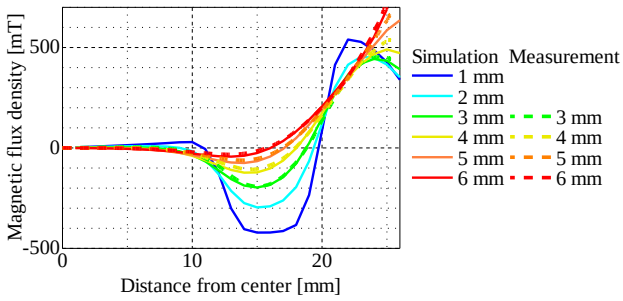

Fig.3.5 Radial component of Magnetic flux density at top of HTS, comparison

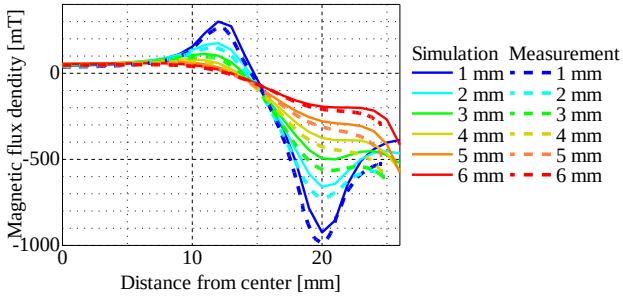

Fig.3.6 Axial component of Magnetic flux density at top of HTS, comparison

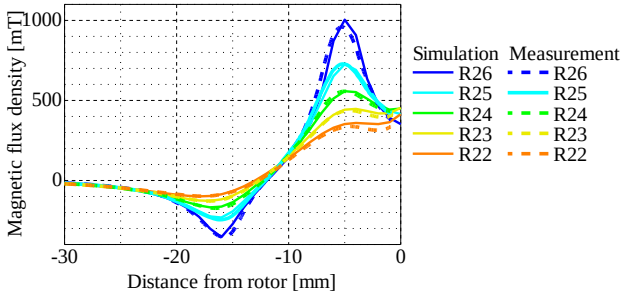

Fig.3.7 Radial component of Magnetic flux density at side of HTS, comparison

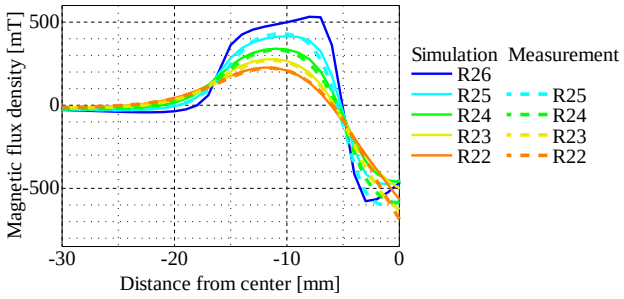

Fig.3.8 Axial component of Magnetic flux density at side of HTS, comparison

For the radial direction component of the measurement results on the HTS side, the measurement result appears to be at a position of -12 mm compared with the simulation result, but the magnitudes almost match. Regarding the axial direction component, the measurement result is closer to the minus side as compared with the simulation result when the position is close to the rotor lower part.

As a cause of these deviations, it is conceivable that the size of the segment magnet is somewhat small, the strength of remnant magnetization of the ring magnet of the magnet is different from the simulation, dimensional error at SMB assembly, etc.

Based on the magnitude criterion of the magnetic flux density, the error was about 7% at the peak and it was judged that the magnetic flux density distribution was obtained almost as the simulation result was obtained.

Subsequently, in order to ascertain to what extent fluctuation in magnetic flux density in the circumferential direction caused by the segment type magnet which is a cause of the rotational resistance of the SMB, the rotor part was attached to the jig and the magnetic flux density was measured while rotating with the ball bearing. The distance from the rotor section at the measurement position is 2 [mm].

A graph of circumferential variation of radial component of magnetic flux density is shown in Fig.3.9 and a graph of circumferential variation of axial component of magnetic flux density is shown in Fig.3.10.

From the measurement results, the variation in the radial direction was about 10 [mT] at the largest R23 and about 20 [mT] at the R23 with the largest variation in the axial direction. This is due to the fact that the fluctuation per cycle is not rotated fixedly around the axis center properly during measurement. Magnetic flux density fluctuation of 16 times period caused by the segment magnet was slightly larger than the simulation result. This is because the size of the segment magnets was slightly smaller in the angular direction than at the time of designing, so it is thought that this is due to the formation of gaps between the segment magnets. However, since this fluctuation is not so large as compared with the magnitude of the magnetic flux density of the magnetic flux converging portion, it is considered that the fluctuation of the magnetic flux density in the circumferential direction does not greatly affect the rotational resistance of the SMB.

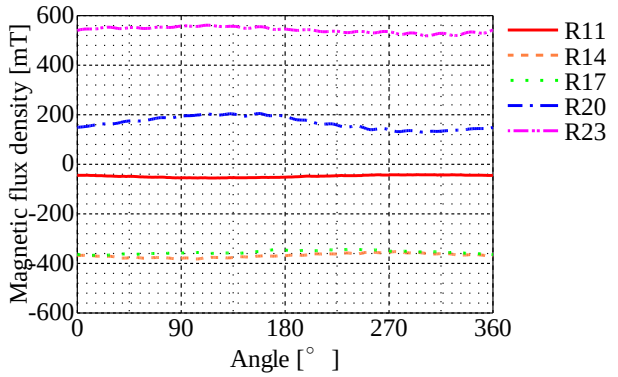

Fig.3.9 Circumferential variation of Magnetic flux density in Radial component, measurement result

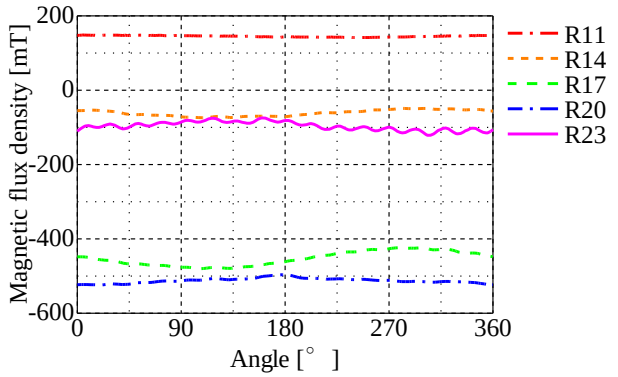

Fig.3.10 Circumferential variation of Magnetic flux density in Axial component, measurement result

3.2 Restoring force generated by SMB

3.2.1 Radial restoring force

In the manufactured SMB, the radial restoring force was measured in order to confirm that the radial instability due to the repulsive magnet could be stabilized by the pinning force by the superconductor. A diagram of the measuring device is shown in Fig.3.11.

First, in order to confirm the unstable characteristics in the radial direction of the repulsion levitation system, the force against the radial displacement in the state where the binding force by the HTS does not work was measured. The distance between the repulsion magnets was changed by changing the height of the repulsion magnet on the stator side.

After fixing the rotor part to the center position, the rotor part was constrained so as not to move in the radial direction except for the roller, and when the rotor part was displaced, the restoring force generated in the radial direction was measured. The displacement was given to the stage by ± 1.5 [mm] in the horizontal direction. Restoring force was measured with a force gauge. The displacement starts from 0 mm and moves to +1.5 mm, -1.5 mm, 0 mm.

Subsequently, the restoring force in the case of constraint by the superconductor was measured.

After fixing the rotor part to the center position, the superconductor was cooled and the rotor part was constrained by the superconductor. When the rotor part was displaced, the restoring force generated in the radial direction was measured. The displacement was given to the stage by ± 1.5 [mm] in the horizontal direction. Restoring force was measured with a force gauge. In any case, the positional relationship between the HTS and the SMB magnetic flux generator on the rotor side is the same.

The measurement result is shown in Fig.3.12. The displacement starts from 0 mm and moves to +1.5 mm, -1.5 mm, 0 mm.

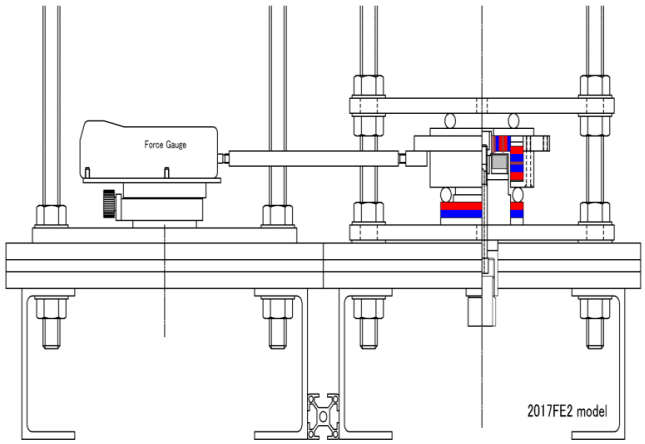

Fig. 3.11 Measurement method of radial restoring force

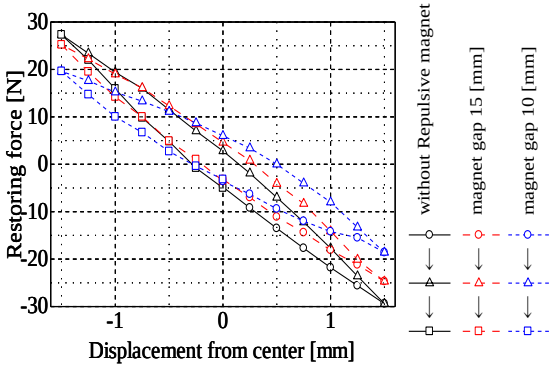

Fig.3.12 Radial restoring force, measurement result

From these results, the restoring force becomes weaker as the repulsive magnet on the stator side gets closer, but it can be seen that the instability of the repulsive levitation system can be canceled. Also, it can be seen that the hysteresis at displacement 0 [mm] does not change so much.

3.2.2 Axial restoring force

In the fabricated SMB, the radial restoring force was measured to confirm the stability in the radial direction. A diagram of the measuring device is shown in Fig.3.13.

The measurement result is shown in Fig. 3.14.

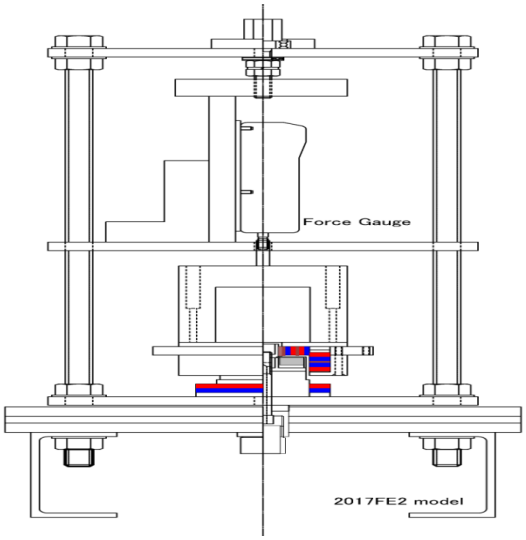

Fig. 3.13 Measurement method of Axial restoring force

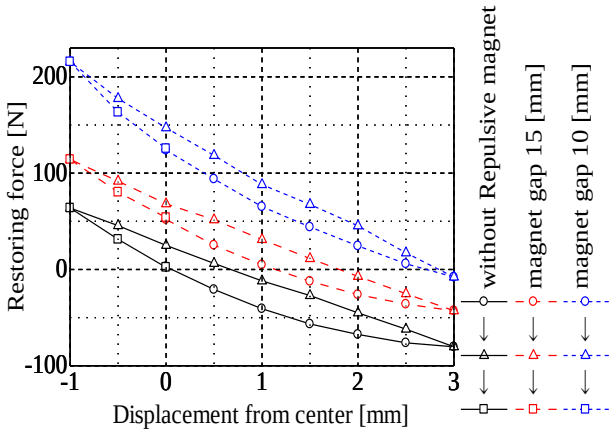

Fig.3.14 Axial restoring force, measurement result

It can be seen that clear graphic nonlinearity appears in each graph because it is a restoring force due to magnetic force. However, it is expected that the driving part of the flywheel this time will behave in a substantially linear manner because it is a structure that does not generate vibratory force in the up and down direction and use in the vicinity of displacement 0 [mm]. In the case where there is a repulsion magnet, since the restoring force at displacement 0 [mm] is a positive value, it indicates that the rotor part moves upward unless a force is constantly applied from above due to the weight of the weight, this indicates that we can support weight of flywheel this time only by repulsive magnet force.

3.2.3 Pitching direction Restoring force and damping force

Fig. 3.15 shows the diagram of the measuring device. After fixing the rotor part to the center position at room temperature using a jig, the superconductor is cooled with liquid nitrogen to constrain the rotor part with the superconductor, the angular response at the time when the fixing of the rotor portion was released and the free vibration was given by applying displacement in the pitching direction was measured by a laser displacement meter.

Fig.3.16. shows the measurement results without repulsion magnets on the stator side.

The measurement result in the case where the distance between the lower end of the ring magnet of the rotor section and the repulsive magnet on the stator side is 15 [mm] is shown in Fig.3.17.

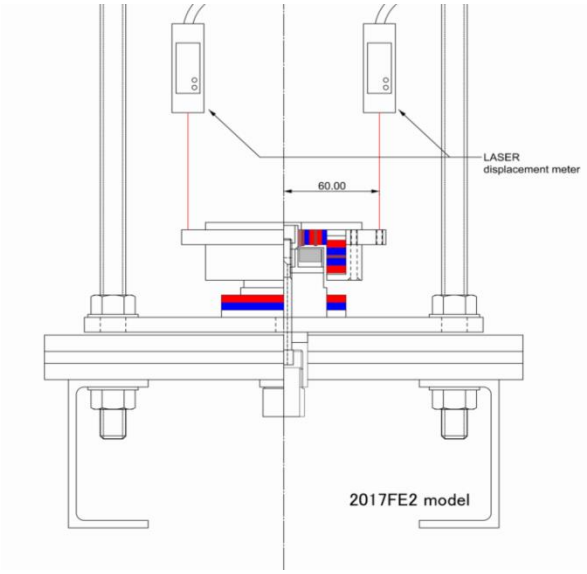

Fig.3.15 Measurement method of pitching vibration

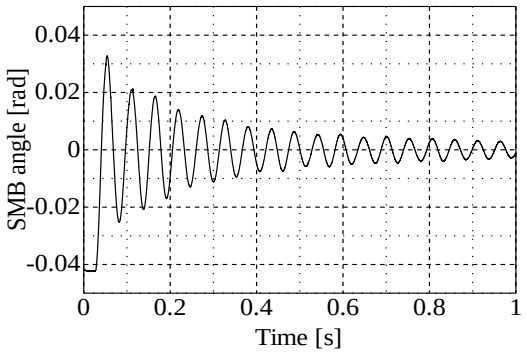

Fig.3.16 Time career reply of angle of SMB without repulsive magnet

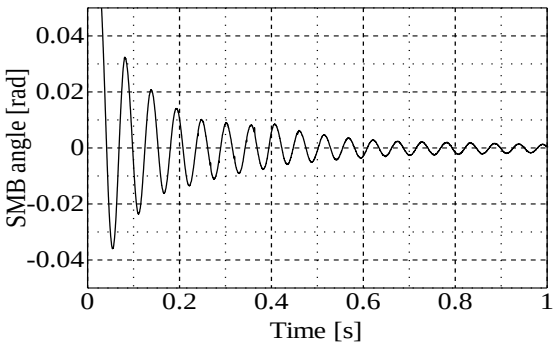

Fig.3.17 Time career reply of angle of SMB with repulsive magnet, gap 15[mm]

From this result, when the repulsive magnet is arranged on the stator side, the restoring force coefficient hardly changes but the damping coefficient becomes large. Actually, this pitching restoring force also has nonlinearity, and the cycle is slightly different depending on the vibration amplitude. When the flywheel is attached, the pitching frequency is about 6.1 [Hz], and it does not resonate at the high speed rotation of the flywheel.

For this reason, it was judged that the characteristics of this SMB's pitching direction restoring force are suitable for flywheel bearings.

3.2.4 Comparison with each axis restoring force of previous study

The restoring force in the radial, axial and pitching directions of the SMB fabricated in this study was compared with the model of previous study. Fig.3.18 shows the structure of SMB produced by the predecessor in the research.

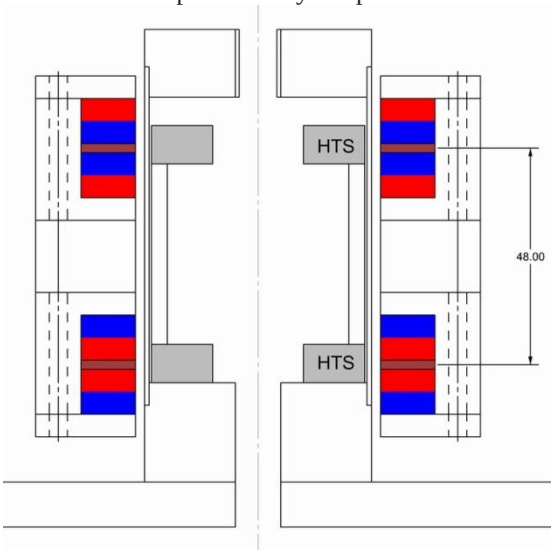

Fig.3.18 SMB model in study of previous research

Table 2.2 measuring result

	Previous model	Present model with repulsive PM gap15mm
Radial restoring force [N/m]	1.8×10^4	1.7×10^4
Axial restoring force [N/m]	4.6×10^4	4.7×10^4
Pitching restoring force [N·m/rad]	27.8	12.8
Total volume of HTSs [m^3]	2.27×10^{-5}	1.14×10^{-5}
Total volume of PMs [m^3]	9.95×10^{-5}	6.48×10^{-5}

Table 2.2 shows the results of comparing the restoring force of each axis, the total high-temperature superconductor (HTS) usage and the total permanent magnet (PM) usage.

The total HTS usage and total PM usage of SMB produced in this research are different from SMB in previous study, compared with the SMB of previous research, the SMB of this study is 0.5 times the total HTS usage and about 0.65 times the total PM usage.

Compared to the SMB in previous study, the SMB in this study is about twice the radial rigidity and axial rigidity, and about 0.9 times the pitching rigidity in this study per the total usage of HTS.

Compared to the SMB in previous research, the SMB in this study was about 1.5 times higher in terms of radial rigidity and axial rigidity, and about 0.7 times in terms of pitching stiffness per PM total usage.

IV. DRIVING EXPERIMENT

4.1 Experimental device specifications

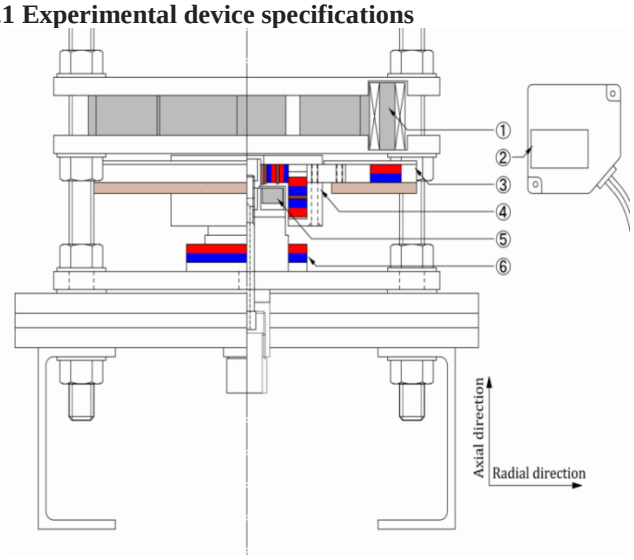

① Driving coil
② Laser displacement meter
③ Rotor flywheel part
④ Rotor SMB part
⑤ HTS
⑥ Stator repulsive PM

Fig.4.1 model of experimental equipment

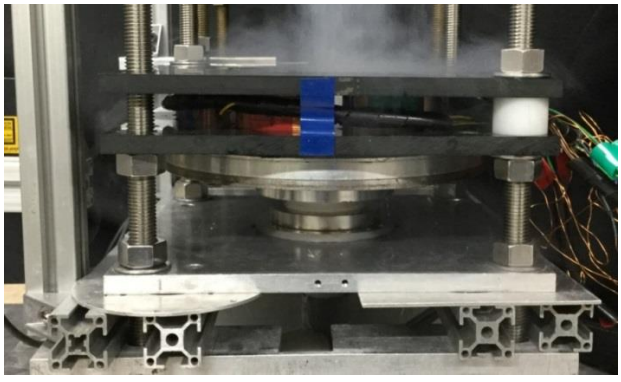

Fig.4.2 Photo of experimental equipment

The whole drawing of the experimental system for driving the flywheel using the SMB manufactured this time is shown in Fig.4.1, and the photo is shown in Fig.4.2.

4.2 The method and result of the experiment

Drive experiments of the flywheel incorporating the SMB manufactured this time were carried out using the experimental equipment shown in Fig.4.1.

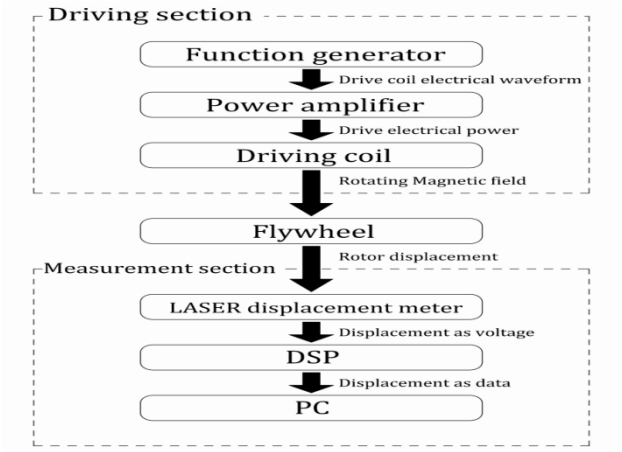

Fig.4.3 scheme of experimental equipment

After fixing the rotor part to the center position using a jig, the HTS is cooled with liquid nitrogen to constrain the rotor part with the superconductor, and after the cooling is completed, the jig is removed to place the flywheel in the air floating state.

In this state, the AC voltage waveform generated by the function generator as shown in Fig. 4.3, was amplified by the power amplifier and applied to the driving coil to generate a rotating magnetic field to synchronously rotate the floating body. The displacement in the radial direction of the floating body at the time of driving was measured with a laser displacement meter and recorded by the PC via the DSP.

Fig.4.4 shows the time change of the frequency of the AC voltage waveform generated by the function generator. The frequency was continuously raised from 0 [Hz] to 500 [Hz] over about 1080 [s]. In the section from 0 [s] to 180 [s], the temporal change of the radial displacement of the floating body obtained by the laser displacement meter is shown in Fig. 4.5, moved by 10 points with respect to the data of sampling frequency 2000 [Hz] It is an average.Fig.4.6 shows a plot of the same frequency and amplitude as axes.

From Fig.4.6, the resonant frequency was about 12 [Hz], and the maximum piece amplitude was about 1.1 [mm] from the time series waveform of the rotor displacement in Fig.4.5. Vibrations are seen even at higher frequencies than the reluctance resonance, but it seems to be caused by the fact that the center of rotation of the SMB and the geometric center of the flywheel do not exactly match.

The maximum rotational speed was 10000 [rev / min], and the estimated rotational energy was about 12 [kJ].

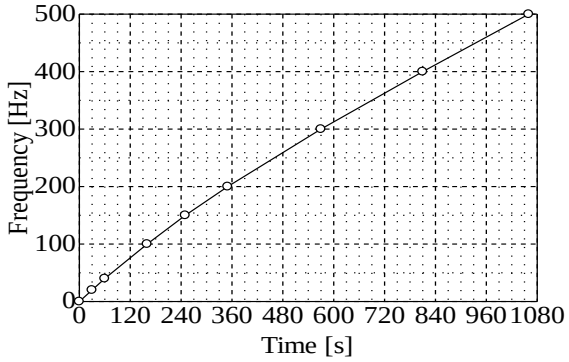

Fig. 4.4 Frequency change of driving coil applied voltage

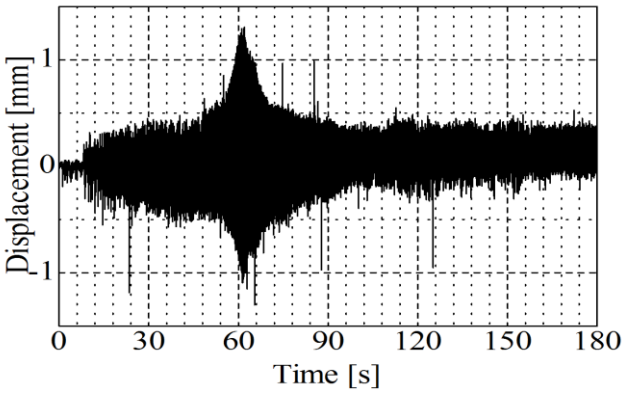

Fig. 4.5 Time series plot of flywheel displacement from 0[s] to 180 [s]

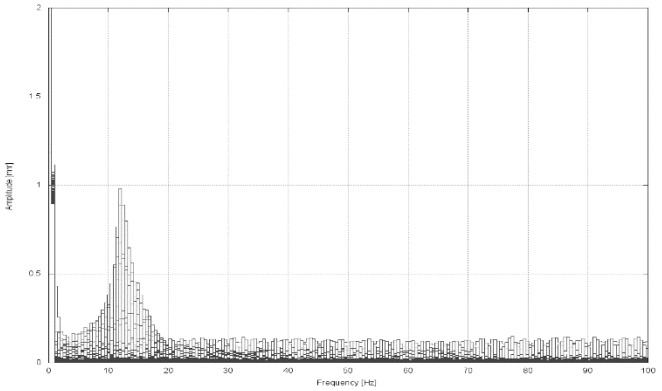

Fig. 4.6 Frequency response of flywheel displacement from 0[Hz] to 100[Hz]

V. CONCLUSION

In this research, we aim to stabilize the radial unstable force generated by repulsion magnet by magnetic flux pinning of superconductor, in charge of axial levitation force required for floating of flywheel by repulsive force of permanent magnet We have developed magnetic bearings using one ring type high temperature superconductor.

The contents of this research are summarized below.

1. We have devised and fabricated an SMB having a repulsive magnetic levitation part utilizing top and side surfaces of a ring type high temperature superconductor for magnetic flux pinning.
2. We confirmed that the unstable force generated by repulsive type magnetic levitation can be stabilized by SMB pinning.
3. Compared with the previous research, even if the usage of superconductor and permanent magnet was halved, equivalent restoring force characteristics were obtained.
4. Comparison of the measurement result of the magnetic flux density distribution generated by the magnetic bearing rotor part in the HTS part with the simulation result confirmed the usefulness of the simulation.
5. It was confirmed that the flywheel using the proposed SMB rotated beyond the dangerous speed without any control, and that it stably buys up to the high speed rotation area.

From the above, we succeeded in stabilizing the magnetically repulsive levitation system with the superconducting magnetic bearing while reducing the amount of high-temperature superconductor used, which is the research purpose.

REFERENCES

[1] K.Nagaya, "Analysis of a high Tc superconducting levitation system with vibration isolation control" IEEE Trans. Magn., Vol.32, No.2, (1996), pp.445-452

[2] K.Nagaya, S.Shuto, "Approximate boundary conditions in a circular conductor and their application to nonlinear vibration analyses of high-Tc superconducting levitation system" IEEE Trans. Magn., Vol.32, No.3, Pt.2, (1996), pp.1888-1896

[3] K.Nagaya, M.Tsukagoshi, Y.Kosugi and M.Murakami, "Vibration control for a high-Tc superconducting non-linear levitation system" Journal of Sound and Vibration, Vol.208, No.2, (1998), pp.299-311

[4] M.Komori, T.Ide, S.Fukata and T.Matsushita, "Vibration suppression of a disk-shaped superconductor with PD control" Cryogenics, Vol.37, No.4, (1997), pp.195-199

[5] S.Sato, K.Sato, K.Fuzihira, M.Hashimoto and K.Miyamoto, "Development of noncontact transport system along vertical guideway using QMG bulk materials" Advances in Superconductivity VII. Proceedings of the 7th International Symposium on Superconductivity (ISS'94), p.2 Vol. (xxii+xvii+1328), (1996), 1251-1254 Vol.2

[6] H.Higasa, F.Ishikawa, M.Shibayama and T.Ono, "A feasibility study of an 8-MWh flywheel type power storage system using oxicide superconductor", Electrical Engineering in Japan, Vol.114, No.7, (1994), pp.20-31.

[7] T.Sugiura, M.Tashiro, Y.Uematsu and M.Yoshizawa, "Mechanical stability of a high Tc superconducting levitation system", IEEE Trans. Appl. Supercond., Vol.7,No.2, (1996), pp.386-389

[8] K.Nagaya, K.Kanno and N.Hayashi, “Control of flywheel system with high-Tc superconducting bearings”, Int.J. of Applied Electromagnetics and Mechanics, Vol.10 (1999), pp.237-247.